

RSC Advances



This is an *Accepted Manuscript*, which has been through the Royal Society of Chemistry peer review process and has been accepted for publication.

Accepted Manuscripts are published online shortly after acceptance, before technical editing, formatting and proof reading. Using this free service, authors can make their results available to the community, in citable form, before we publish the edited article. This *Accepted Manuscript* will be replaced by the edited, formatted and paginated article as soon as this is available.

You can find more information about *Accepted Manuscripts* in the [Information for Authors](#).

Please note that technical editing may introduce minor changes to the text and/or graphics, which may alter content. The journal's standard [Terms & Conditions](#) and the [Ethical guidelines](#) still apply. In no event shall the Royal Society of Chemistry be held responsible for any errors or omissions in this *Accepted Manuscript* or any consequences arising from the use of any information it contains.

CARBON NANOTUBE BASED 3-DIMENSIONAL HIERARCHICAL FIELD EMITTER STRUCTURE

Gaurav Mittal^a, Mamta Khaneja^b, Krishna Saini^a, Indranil Lahiri^{a, c, *}

^aCentre of Nanotechnology, Indian Institute of Technology Roorkee, Roorkee-247667, INDIA

^bSolid State Physics Laboratory, DRDO, New Delhi-110054, INDIA

^cNanomaterials and Applications Lab., Department of Metallurgical and Materials Engineering,
Indian Institute of Technology Roorkee, Roorkee-247667, INDIA

* Corresponding author: E-mail: indrafmt@iitr.ac.in, Ph: +91-1332 285261, Fax: +91-1332 285243

ABSTRACT: Carbon nanotubes (CNT) are known to offer exciting electronic, electrical, mechanical and chemical properties and have found their way in a variety of applications. Field emitter is one such application in which the use of CNTs is widely appreciated. High current density field emitters with good stability have been in focus of many researchers for more than a decade. In the present study, a 3-Dimensional (3D) hierarchical structure of field emitter has been demonstrated. Copper oxide (CuO) nanotubes and nanorods were synthesized directly on a copper foil substrate using a simple, easy to scale-up chemical process and CNTs were grown on these CuO nanostructures. A comparative study of field emission behaviour of these emitters, along with its corresponding 2-Dimensional (2D) structure i.e. CNTs grown on copper foil, was performed. The basic idea behind developing the 3D architecture was to enhance the surface area available for CNT growth, so that higher emission current can be achieved without increasing foot-print of the field emitter device. Emission current density was measured to be 0.87 mA/cm², 3.11 mA/cm² and 0.63 mA/cm² respectively, for CNTs on copper foil, CNTs on CuO nanotubes and CNTs on CuO nanorods.

KEYWORDS: Carbon nanotubes, field emission, 3-Dimensional architecture, emission current density.

1. INTRODUCTION

Field emitters have a wide range of applications in field emission displays¹, microwave amplifiers², x-ray sources³, electron microscopes⁴, satellite propulsion (hall thrusters)⁵ etc. High current density field emitters with good stability are appearing as necessity for most of these applications. One dimensional

nanostructure such as nanorods, nanowires, nanotubes, nanofibres has been explored extensively for field emission application owing to their unique properties like small radius of curvature at tip and high aspect ratio. Among these one dimensional nanostructures, carbon nanotubes (CNTs) were investigated most extensively. They offer almost all the structural features and properties required for a good field emitter i.e. high aspect ratio, high conductivity, high mechanical strength, thermal stability and chemical inertness⁶⁻¹⁰. Apart from CNTs, different nanostructures of metals like silver (Ag) nanorods¹¹, gold (Au) nanowires¹², Cu nanorods¹³ and nanowires/nanotubes of metallic oxides like ZnO¹⁴, TiO₂¹⁵, CuO^{16,17} have also demonstrated promising field emission characteristics.

High emission current density has been one of the main focus areas in development of next-generation emitters. Implementation of 3-D architecture may be a way out in this situation, when conventional 2-Dimensional architecture (with CNTs grown on flat surface) failed to generate such high current density. Increasing spatial density of CNTs could be an option to increase current density. However, excessive and continuous increase in emitter density leads to screening effect which rather decreases the field emission efficiency. The main purpose of using 3-Dimensional architecture is to enhance the effective surface area available for CNT growth (without affecting foot-print area of the device) so that emitter density can be enhanced and screening effect could also be avoided. Figure 1 shows schematic of the process of creating 3-D architecture and availability of more surface area for growth of CNTs. While in the 2-D architecture, only topmost surface is available for CNT growth, in 3-D architecture, surface area is enhanced due to presence of some structural features on top surface. In recent years, different varieties of 3-D emitter structures have been reported by many research groups¹⁸⁻²¹.

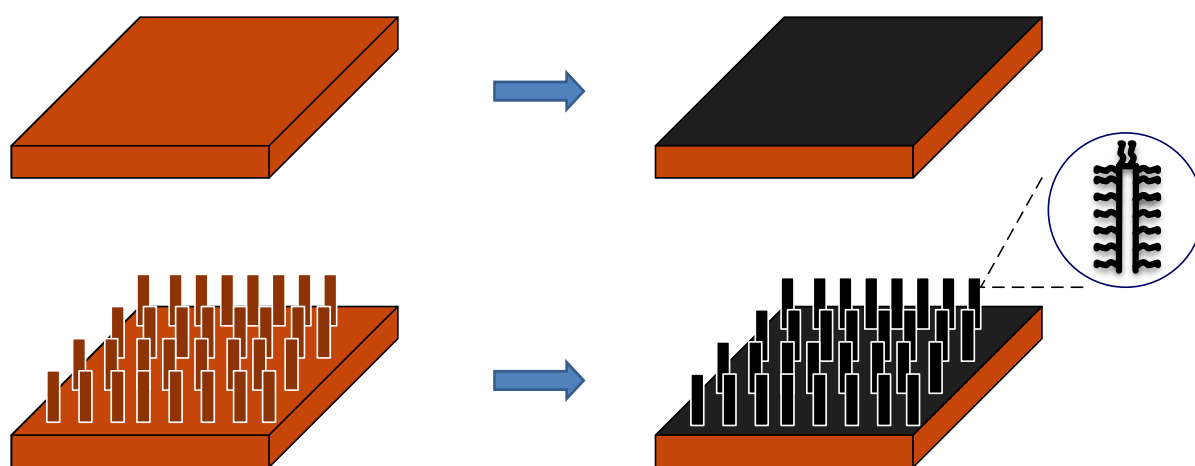


Figure 1. Schematic diagram showing comparison of surface area available for CNT growth in 2-D (top) and 3-D (bottom) architecture.

In the present study, a 3-dimensional hierarchical structure of field emitter was produced to obtain high current density. In these field emitters, CuO nanostructure-CNT hierarchical field emission array

on copper foil was used. The substrate for these field emitter devices was chosen to be copper, because of its high electrical conductivity (among metallic conductors, Cu (5.800×10^7 Siemens/m) is second to Ag (6.287×10^7 Siemens/m) only, in electrical conductivity⁷) and its easy availability. CNT emitters on copper substrate have been known to offer much better field emission properties, as compared to other metallic or semiconducting substrates⁷. In the present study, nickel was chosen to be the catalyst for CNT growth, again considering its higher electrical conductivity compared to other conventional catalyst materials²². In order to prepare the hierarchical structure, the structure chosen should have compatibility with copper, some kind of conductivity and should be processed easily. Cupric oxide (CuO) was selected to be this material, as it is a p-type semiconductor with a band gap of 1.2 eV²³ and CuO nanostructures can easily be synthesized directly on copper foil by simple, easy to scale-up chemical processes. Moreover, various CuO nanostructures are known to offer good field emission properties^{16, 17, 24, 25}. Thus, selection of materials in the present study was dictated with the aim of developing a field emitter device with better emission characteristics and which can be processed by a simple and easy-to-scale-up technique.

The hierarchical field emitter structure was fabricated by a two-step process. First, CuO nanostructures were grown on a copper foil by chemical method. Then CNTs were synthesized over it using thermal chemical vapour deposition (CVD). To the best of authors' knowledge, this Cu-CuO nanostructure-CNT hierarchical structure was demonstrated for the first time for field emitter application. Field emission behaviour was compared among samples with CNTs grown on pure copper foil (i.e. a 2-D structure) and CNTs grown on CuO nanorods (referred as CuO-NR) and CuO nanotubes (referred as CuO-NT), which are considered as 3-D structures.

2. EXPERIMENTAL PROCEDURE

2.1 Synthesis of CuO nanotubes

CuO-NT structure was synthesized following a modified version of the chemical route proposed by Zhang et al.²³. Solutions of sodium hydroxide (NaOH) (10 mol dm^{-3}) and ammonium persulfate ($(\text{NH}_4)_2\text{S}_2\text{O}_8$) (1 mol dm^{-3}) were prepared by dissolving NaOH (98% pure) and $(\text{NH}_4)_2\text{S}_2\text{O}_8$ (98% pure), respectively, in deionized (DI) water. Then, 7.5 ml of the NaOH solution was mixed with 19.5 ml DI water to prepare an alkaline solution. A piece of pure copper foil (99.9% pure) of size $15 \times 15 \times 0.2 \text{ mm}^3$, was bath sonicated in 50% HCl and then washed with acetone and DI water to remove impurities. One side of copper foil was protected with adhesive tape. It was then immersed in the solution prepared above. Finally, 3 ml of $(\text{NH}_4)_2\text{S}_2\text{O}_8$ solution was added to this reaction chamber. The entire reaction chamber was kept in a beaker containing ice and placed in refrigerator, to control

the kinetics of CuO-NT formation. After 7 hours, the copper foil was taken out of the solution and washed repeatedly with DI water and dried in air.

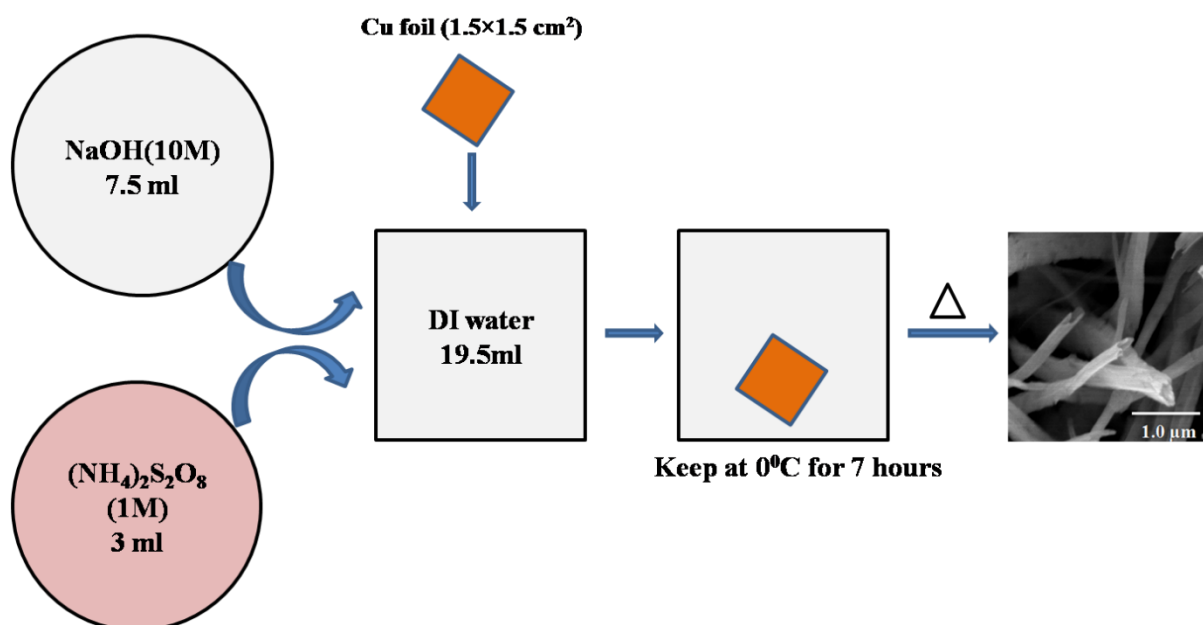


Figure 2. Schematic representation of synthesis of CuO nanotubes obtained by immersing copper foil into a solution of sodium hydroxide and ammonium persulphate for 7 h and thereafter giving heat treatment at 60°C for 2 h, then at 120°C for 4 h and finally at 180°C for 6 h in N₂ atmosphere.

The dried samples were then heat treated in N₂ atmosphere. The samples were kept in an alumina boat and placed in centre of quartz tube furnace. N₂ gas was purged for 10 minutes to flush the tube. Samples were heated first at 60°C for 2 hours, then at 120°C for 4 hours and finally at 180°C for 6 hours in N₂ atmosphere. The whole process is demonstrated in figure 2 with the help of a schematic.

2.2 Synthesis of CuO nanorods

CuO-NR structure was grown on copper foil by a simple chemical method as reported by Xue et al.²⁶. Copper foil (15 × 15 × 0.2 mm³) was bath sonicated in 50% HCl for 10 minutes and then washed with DI water to remove surface impurities. One side of copper foil was protected with adhesive tape. A solution was prepared by mixing 1 ml ammonia and 80 mg NaOH in 400 ml of DI water. The washed copper foil was immersed into the solution prepared and kept at room temperature. The samples were taken out after 7 days and washed repeatedly with DI water to remove surface impurities. Dried samples were then annealed at 200°C for 2 hours in N₂ atmosphere. Figure 3 shows schematic of the whole synthesis process of CuO-NR growth.

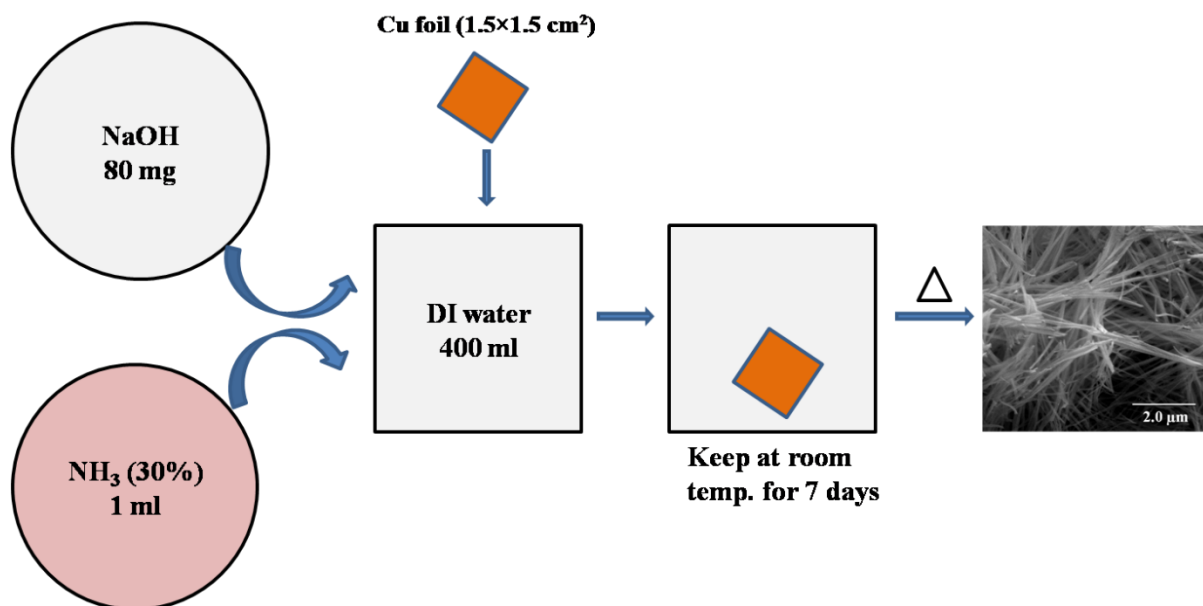


Figure 3. Schematic representation of synthesis of CuO Nanorods on copper foil by immersing it in a solution of sodium hydroxide and ammonia for 7 days and thereafter giving heat treatment at 200°C for 2h in N₂ atmosphere.

2.3 Synthesis of CNTs

CNTs were grown on pure copper foil, CuO NR structure and CuO NT structure by thermal chemical vapour deposition (CVD) method. A solution was prepared by mixing 42 mg nickel acetate (98% pure) to 10 ml of ethanol²⁷. Dip coating method was used to deposit catalyst layer onto substrate. During dip coating, substrate was dipped into the solution for 5 minutes and then dried in air for 10 minutes. This process was repeated 3 times so that sufficient catalyst could be deposited over the substrate. Catalyst deposited samples were placed in an alumina tray and inserted into CVD chamber. The chamber was flushed by purging argon gas for 10 minutes. Samples were heated to temperature range of 700-750°C under the flow of 500-1000 sccm of argon and after reaching the CVD growth temperature, acetylene was flown at rate of 500 sccm for 10 minutes. Finally, the samples were slowly cooled to room temperature under constant flow of Ar gas. The same procedure was repeated for all three types of samples.

2.4 Characterization

The surface morphologies and phase of the as-grown CuO-NTs and -NRs were characterized using scanning electron microscope (SEM) and X-ray diffraction (XRD), respectively. All XRD patterns were analyzed with X'Pert Highscore software. Brunauer-Emmett-Teller (BET) method, with N₂ as adsorbate, was used to quantify surface area of CuO-NT and -NR structures. For this purpose, CuO nanotubes and nanorods were scratched out from copper substrate. The surface and morphology of as-

synthesised CNTs was characterized by SEM, Raman spectroscopy (Invia Renishaw Raman spectrophotometer with Ar laser, having wavelength of 514 nm) and TEM (FEI TECHNAI G2 and JEOL 2100 UHR-TEM) with operating voltage of 200 keV. For TEM observation, a dispersion of CNTs (scrapped out from the sample surfaces) in 5 mL acetone was used, which was bath sonicated for 10 minutes and 10-20 μ l of it was dropped onto copper grids. Field emission tests were performed in parallel plate diode configuration. In the field emission measurement set-up, CNT-based samples mounted on a copper plate, fixed to a stainless steel base plate, acted as a cathode. A stainless steel disk mounted on the same fixture acted as the anode. Typical anode to cathode spacing was maintained at 500 μ m. The complete diode-assembly was kept inside a vacuum chamber, which was evacuated to a base pressure of $\sim 1 \times 10^{-6}$ torr using a turbo-molecular pump backed by mechanical pump. This level vacuum was maintained for all field emission tests. A Gamma 3 kV dc power supply was used to apply high voltage to the test device.

3 RESULTS AND DISCUSSION

3.1 CuO nanotubes and CuO nanorods

As-grown CuO nanotubes and nanorods were characterised initially by X-ray diffraction (XRD) to identify the phases formed. Figure 4 (a) shows XRD pattern of as-synthesized CuO nanotubes. Two low-intensity diffraction peaks matched well with available data of monoclinic CuO (JCPDS 00-001-1117), having lattice constants $a = 4.653 \text{ \AA}$, $b = 3.410 \text{ \AA}$ and $c = 5.108 \text{ \AA}$. Comparing with this JCPDS data, peaks at 35.74 and 38.96 could be attributed to (-1 1 1) and (1 1 1) planes of CuO, respectively. Other peaks of CuO were not visible as they have much less intensity. Other three peaks, present in Figure 4(a) at 2θ values of 43.64, 50.75 and 74.43, were due to copper substrate.

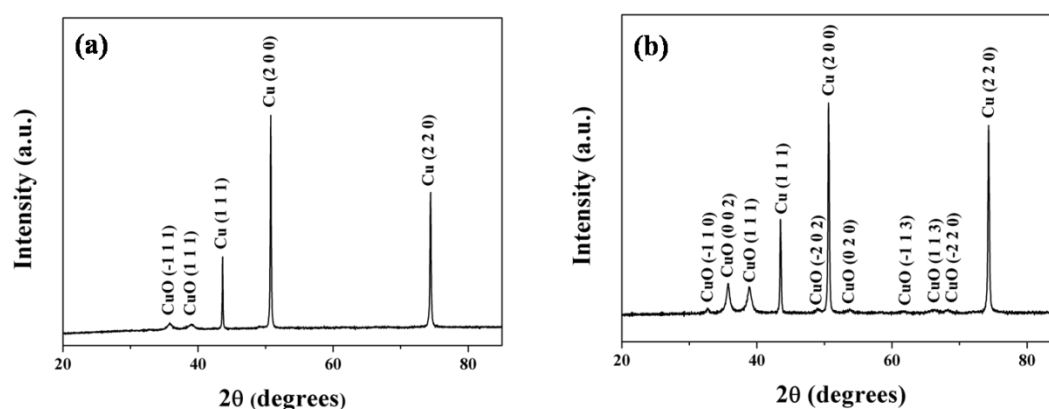


Figure 4. XRD peak pattern of samples (a) CuO nanotubes and (b) CuO nanorods.

Figure 4 (b) shows XRD pattern of CuO nanorods characterized after annealing. The peaks at 32.74, 35.74, 38.83, 49.04, 53.80, 61.67, 67.95 and 68.16 corresponding to (-1 1 0), (0 0 2), (1 1 1), (-2 0 2), (0 2 0), (-1 1 3), (1 1 3) and (-2 2 0), respectively were matched closely with synthetic tenorite (another variety of monoclinic CuO) structure (JCPDS 00-045-0937) with lattice constants $a = 4.6853 \text{ \AA}$, $b = 3.4257 \text{ \AA}$ and $c = 5.1303 \text{ \AA}$. All the remaining 2θ peaks (43.48, 50.59 and 74.29) belong to copper substrate.

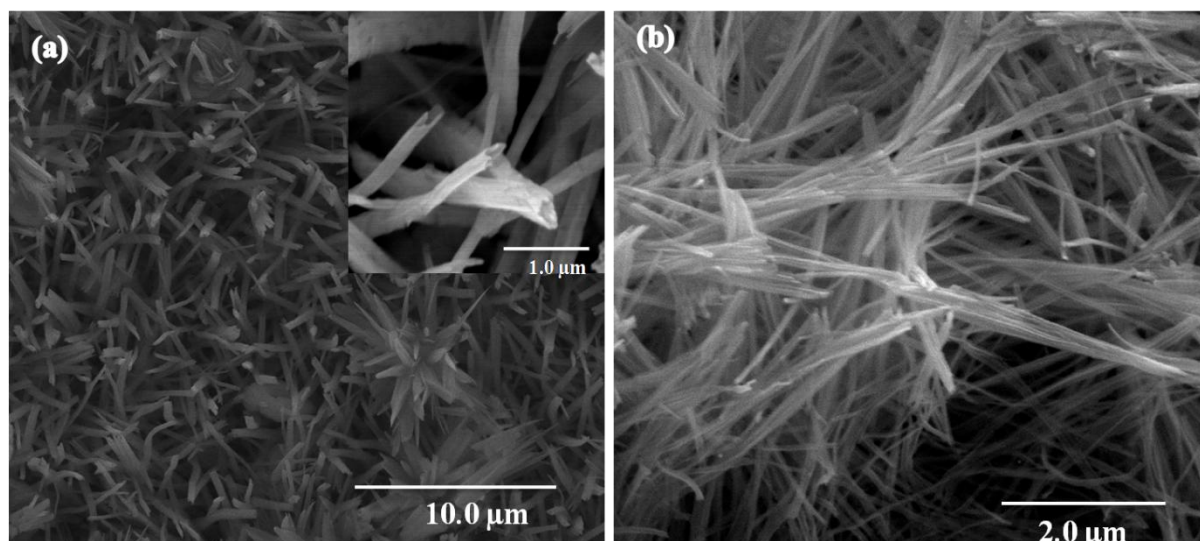


Figure 5. FE-SEM micrographs of the samples. (a) CuO nanotubes (inset is the higher magnification image of the same sample showing nanotube structure formation) and (b) CuO nanorods.

The morphology and structure of CuO-NTs and CuO-NRs, as characterised by FE-SEM, are shown in figure 5. Figure 5(a) shows micrograph of the CuO nanotubes which were uniformly grown on the surface of copper foil. CuO nanotubes were found to be vertically erected on the substrate. The mean diameter of the nanotubes was measured to be $315 \pm 83 \text{ nm}$ and lengths of several micrometers. Higher magnification SEM image (inset of figure 5(a)) clearly shows the nanotube formation. The lower reaction temperature (0°C), used for synthesis of CuO-NTs, decreases the reaction rate and the surface of the copper foil was uniformly covered with the characteristic blue film of $\text{Cu}(\text{OH})_2$ ²³. On annealing, $\text{Cu}(\text{OH})_2$ is converted to CuO. Figure 5 (b) presents low magnification SEM image of the CuO nanorods. In contrast to CuO-NTs, nanorods were observed to be randomly oriented and were also not uniformly distributed over the whole substrate.

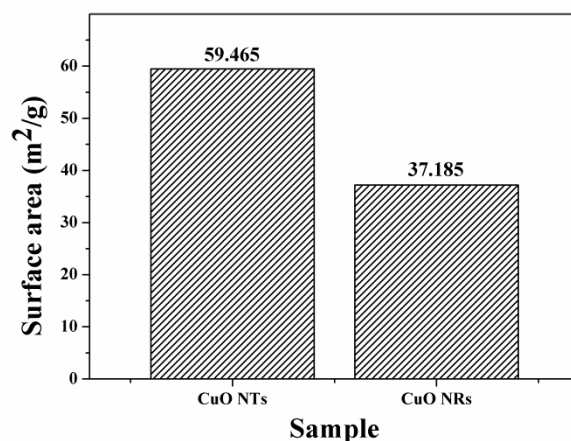


Figure 6. BET Surface area comparison of CuO NTs and CuO NRs.

Surface area of the as-synthesized nanostructures was calculated using Brunauer-Emmett-Teller (BET) method. CuO NTs and NRs were grown on same size of copper foil samples i.e. $1.5 \times 1.5 \text{ cm}^2$ and scratched out of substrate surface to measure surface area. The calculated surface area was measured to be $59.465 \text{ m}^2/\text{g}$ and $37.185 \text{ m}^2/\text{g}$ for CuO NTs and CuO NRs, respectively (figure 6), as compared to a very low value of $5.61 \text{ cm}^2/\text{g}$ for 2-D copper foil.

3.2 Synthesis of carbon nanotubes on different substrates

Figure 7 shows the FE-SEM images of the as-synthesized CNTs on different samples. Figure 7(a) shows randomly oriented multiwall carbon nanotubes (MWCNT) grown on pure copper foil. The mean diameter of these MWCNTs was measured to be $48 \pm 6 \text{ nm}$, as shown in the diameter histogram plot (figure 7(d)). CNTs were also grown on CuO NT and NR structures using same CVD parameters, as used for pure copper foil. FE-SEM micrographs of these are shown in figure 7(b) and (c), respectively. Diameter of these MWCNTs was measured to be $89 \pm 23 \text{ nm}$ and $69 \pm 7 \text{ nm}$ for CuO NTs and CuO NRs, respectively, as represented by histogram plots in figure 7(e) and (f).

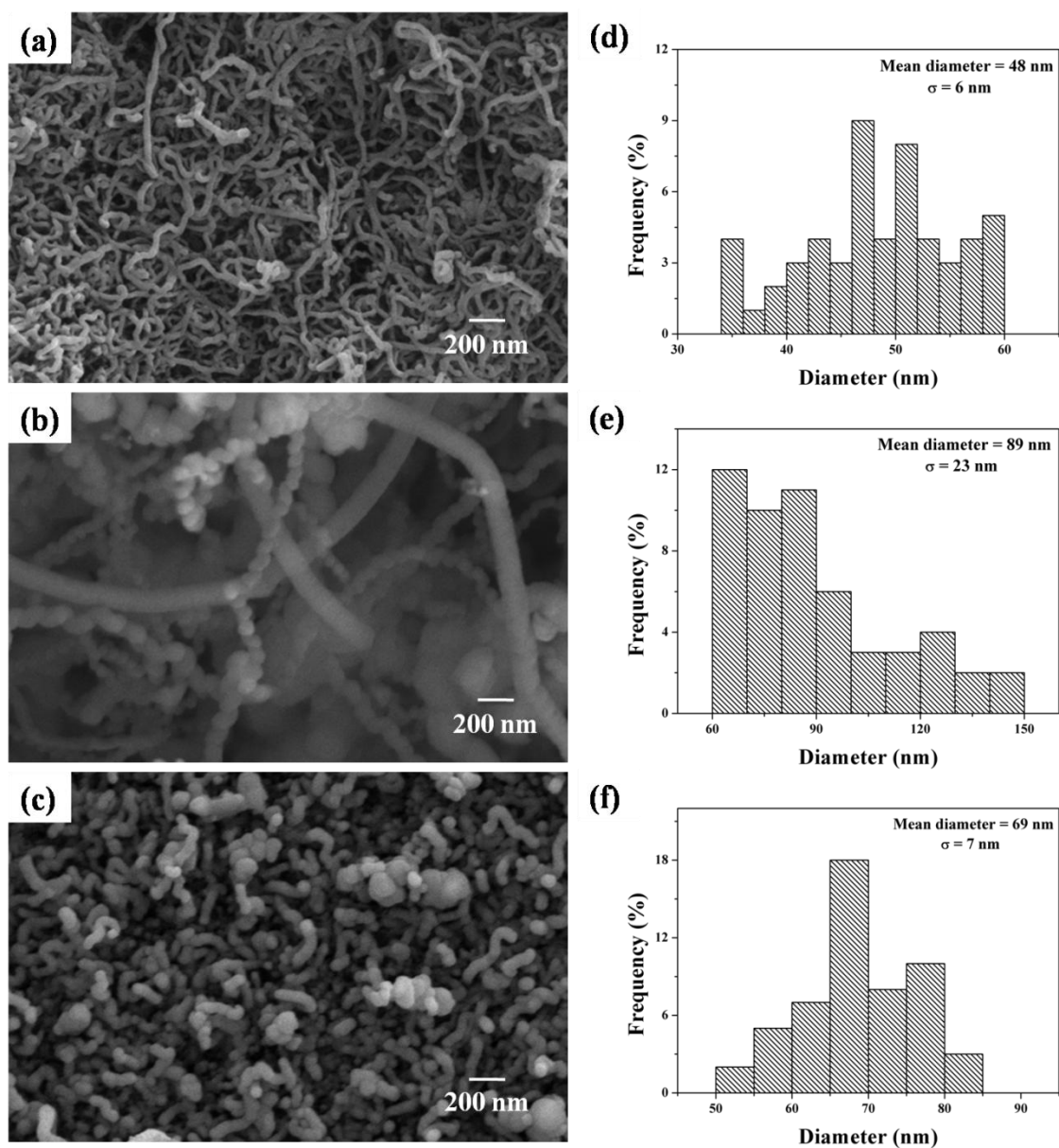


Figure 7. FE-SEM images of CNTs grown on (a) copper foil, (b) CuO NTs and (c) CuO NRs; diameter distribution histograms of CNTs grown on (d) copper foil, (e) CuO NTs and (f) CuO NRs.

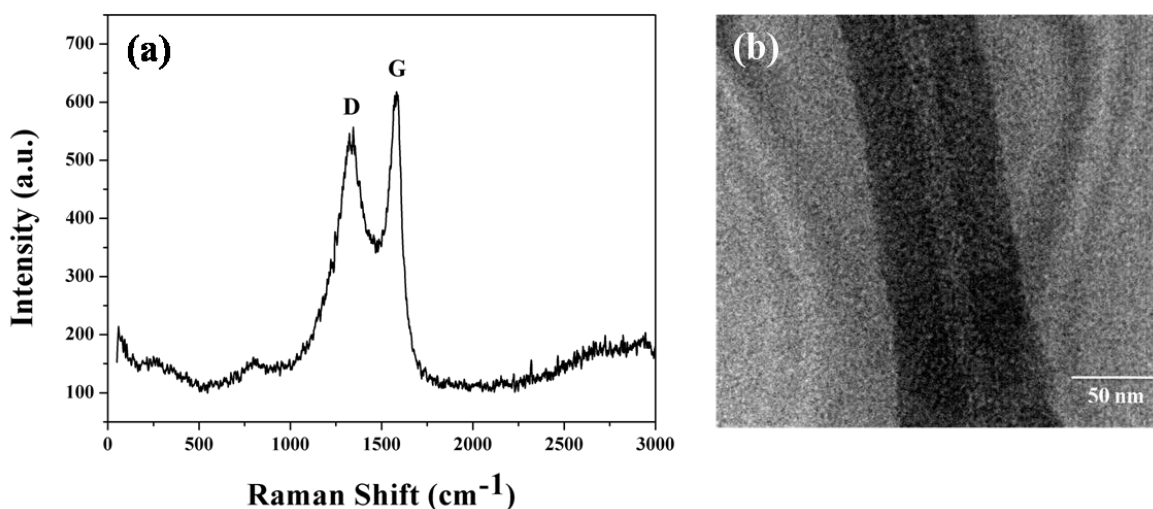


Figure 8. (a) Raman spectra of the MWCNTs on copper foil with characteristic peaks at 1346.71 cm^{-1} and 1590.89 cm^{-1} , (b) a representative TEM image of the as-synthesized CNT.

To better understand the nature of CNT structures, TEM and Raman spectroscopy was performed. Figure 8(a) shows Raman spectra of carbon nanotubes grown on copper foil. First-order Raman spectra of all graphite like materials, including MWCNTs, show peaks around 1580 cm^{-1} (G-band, from graphite like sp^2 bonds) and 1350 cm^{-1} (D-band, from diamond like sp^3 bonds)²⁸. In the present study, peaks were shifted to 1590.89 cm^{-1} and 1346.71 cm^{-1} , indicating significant amount of crystallinity and defects present in the material respectively. Structural purity of the CNT materials is most popularly characterized by I_D/I_G peak ratio. High ratio ($I_D/I_G = 1.113$) in the present study indicates high defect density in MWCNTs structure. Raman spectra for the sample did not show any peak at RBM band depicting absence of SWCNTs. TEM image, shown in figure 8(b), throws direct light on the presence of clear-cut tubular structure in these MWCNTs.

3.3 Field emission characteristics

All field emission tests were performed under DC bias. Field emission characteristics of these MWCNTs based samples are presented in figure 9. Figure 9(a) shows current density vs. applied field (J-E), while figure 9(b) presents an enlarged view of this curve to identify the turn-on fields of these emitters. Fowler-Nordheim (F-N) plots are presented in figure 9(c).

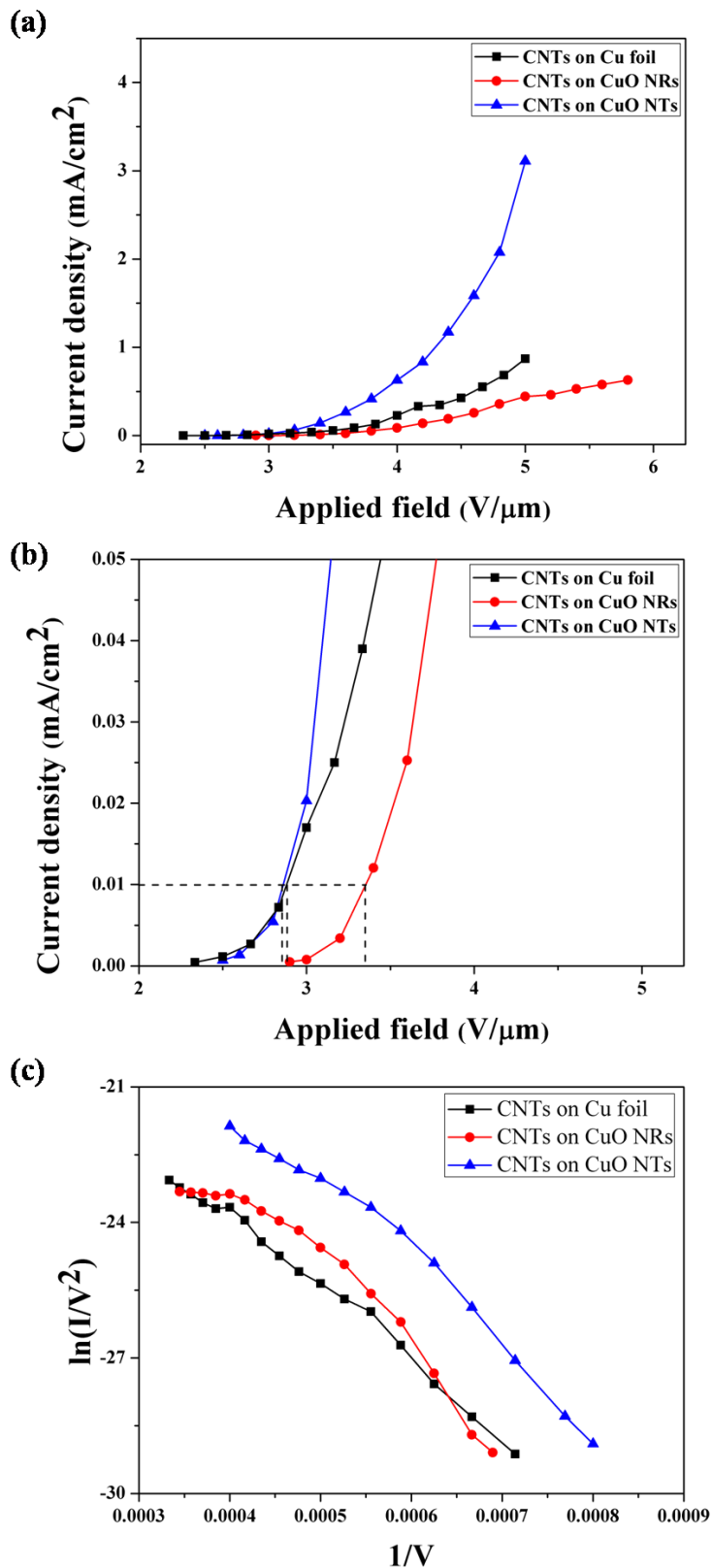


Figure 9. Field emission characteristics of all the emitter structures. (a) Emission current density, (b) turn-on field and (c) Fowler-Nordheim plot for CNTs on copper foil (Black Square), CNTs on CuO NTs (blue triangle) and CNTs on CuO NRs (red circle).

The turn-on field (defined as the electric field required to achieve emission current density of 10 $\mu\text{A}/\text{cm}^2$) was found to be 2.88 $\text{V}/\mu\text{m}$, 2.86 $\text{V}/\mu\text{m}$ and 3.36 $\text{V}/\mu\text{m}$ for CNTs grown on pure copper foil, CuO nanotubes and CuO nanorods, respectively. In this respect, CNTs-CuO NR-Cu emitter structure was found to be much worse than the other two structures – a behaviour which can be related to highly inhomogeneous growth of CuO NRs. However, nearly straight line nature of all F-N plots, shown in figure 9(c), indicates that the emission mechanism, for all the emitters, was essentially electron tunnelling. Field enhancement factor (β) was calculated using Fowler-Nordheim (F-N) equation i.e. $I = (aA\beta^2 E^2 / \phi) \exp[-b\phi^{3/2} / \beta E]$ ²⁷. From the F-N plot, field enhancement factor has been calculated as 4841, 4408 and 4540 for CNTs grown on pure copper foil, CuO nanotubes and CuO nanorods respectively. This observation can be reconfirmed from calculations shown by Xu *et al*³⁶ which shows decrement in field enhancement factor as the radius of MWCNT increases.

Sample	Surface area (m^2/g)	CNT diameter (nm)	Turn-on field ($\text{V}/\mu\text{m}$)	Emission current density (mA/cm^2)	Field enhancement factor (β)
CNTs on Cu foil	0.0056	48 \pm 6	2.88	0.87	4841
CNTs on CuO Nanotubes	59.465	89 \pm 23	2.86	3.11	4408
CNTs on CuO Nanorods	37.185	69 \pm 7	3.36	0.63	4540

Table 1. Table showing surface area, CNT diameter, turn-on field, emission current density and field enhancement factor for CNTs grown on copper foil, CuO NTs and CuO NRs.

Emission current density was recorded to be 0.87 mA/cm^2 , 3.11 mA/cm^2 and 0.63 mA/cm^2 at applied electric fields of 5 $\text{V}/\mu\text{m}$, 5 $\text{V}/\mu\text{m}$ and 5.8 $\text{V}/\mu\text{m}$ for CNTs on copper foil, CuO nanotubes and CuO nanorods (0.44 mA/cm^2 at 5 $\text{V}/\mu\text{m}$), respectively, as shown in figure 9(a). It was also observed that the emission current density from CNTs grown on CuO NTs was much higher than other samples, which may be related to the large surface area of CuO nanotubes (as confirmed by BET, Figure 6). Larger surface area of CuO-NTs prompted for growth of more number of CNTs grown on them, which in turn led to higher emission current density. On the other hand, current density from CNTs grown on CuO NRs was very low, even lower than the conventional 2-D emitter structure. This observation may be related to the in-homogeneity of CuO NRs structure, which led to non-uniform growth of CNTs and hence, a poor field emission response.

The variation in emission current from CNT-CuO NT-Cu and CNT-CuO NR-Cu samples can also be correlated with the diameter distribution of grown CNTs. Although field enhancement factor decrease as radius of CNT increase as calculated by Xu *et al*³⁶, but in case of large radii CNTs, emission current increases as the radius of the MWCNTs increases, due to increment in emitting area³⁷. Hence the CNT-CuO NT-Cu emitter, which have largest radii, emit maximum current among the three structures studied. Even if MWCNTs were of same size, CNT-CuO NT-Cu emitter is anticipated to demonstrate better emission properties, simply owing to its higher surface area and more number of CNT emitters being present in that structure.

Results obtained in the present study show best emission properties from CNT-CuO NT-Cu emitter structure. Turn-on field (2.86 V/ μm) obtained from this sample was better than many other emitter structures, including another variety of hierarchical structure of ZnO nanoneedles on ZnO nanofiber (Table-2). However, turn-on field was found to be more than most of the nanostructured carbon material based emitters. This observation can be related to the presence of CuO in our emitter structure, which is known to be a p-type semiconductor, offering higher resistance than nanostructured carbon materials (CNTs or graphene). On the other hand, emission current density, obtained from our sample, was found to be much higher than most of the emitters, as shown in Table-2. It can be recalled here that the aim of the present study was to get high emission current density from hierarchical emitter structure, which appears to be fulfilled. However, there is ample opportunity to further improve the emission current density and efforts are underway to address this issue. Present study clearly proves the effectiveness of hierarchical structure over conventional 2-dimensional emitters. Further, the simplicity of the process to prepare this hierarchical emitter structure makes it a promising emitter material for industrial application. Moreover, the processing technique involves direct synthesis of CuO-NTs on copper foil and direct growth of CNTs onto it. All these direct growth processes ensures that the emitters are bonded well with the substrate, which is an important factor for life time of any device²⁸.

Sr. No.	Material	Turn on field	Emission Current Density	Reference
1	Ar plasma treated FLG sheet on Si	2.23 V/ μm	1.3 mA/cm ²	29
2	N-doped graphene on Si substrate	0.6 V/ μm	10 $\mu\text{A}/\text{cm}^2$	30
3	MWCNT on Cu substrate	0.6 V/ μm	Total emission current = 1.5 mA	31
4	B-doped CNT ($7 \times 7 \text{ mm}^2$) on Si substrate	3 kV	Current density is 4A/cm ² for total emission current = 1 μA	32
5	SWCNT grown on textured Si substrate	1.3-2.4 V/ μm at 1 $\mu\text{A}/\text{cm}^2$	0.1-1.2 mA/cm ²	33
6	BN Nanotube deposited on as grown Graphite Nanofibre	0.72 V/ μm	Total emission current = 89 μA	34
6	BN Nanotubes on Si substrate	8.3 V/ μm	-	35
7	ZnO Nanoneedles on ZnO Nanofibre	4.8 V/ μm	-	21
8	3-D Metal-Graphene-Nanotube	0.26 V/ μm	12.67 mA/cm ²	19

Table 2:- Field Emission characteristics of various field emitters. (Turn on field value is defined at 10 $\mu\text{A}/\text{cm}^2$ unless otherwise mentioned)

4. CONCLUSION

In the present study, a 3-Dimensional hierarchical field emitter structure has been fabricated successfully in which CNTs has been synthesised on CuO nanotubes and nanorods structures, which in turn was synthesized directly onto copper foil. A comparative study between CNTs on copper foil (i.e. 2-D structure) and CNTs on CuO NTs and NRs (i.e. 3-D structure) showed great promise of 3-D structures. The hierarchical structure having CNT-CuO NT-Cu registered more than 250% increase in emission current density as compared to CNTs directly grown on copper foil. Enhancement in emission current density of 3-D hierarchical structure was related to higher surface area of CuO-NT structure and its uniform distribution over copper foils.

5. ACKNOWLEDGEMENT

G.M. would like to thank Dr. Anil Kumar, Head, Department of Chemistry, IITR for allowing to use the Raman spectrometer and Dr. P. Jeevanandam, Department of Chemistry, IITR for allowing to use BET. G.M. would also like to thank Head, Institute Instrumentation Centre, IITR for allowing access to various analytical facilities. M.K. wishes to thank nanotechnology group of SSPL for providing support in field emission tests. This study was funded by IL's IIT Roorkee faculty initiation grant (Grant no. FIG/100612).

6. REFERENCES

- 1 W.B. Choi, D.S. Chung, J.H. Kang, H.Y. Kim, Y.W. Jin, I.T. Han, Y.H. Lee, J.E. Jung, N.S. Lee, G.S. Park, J.M. Kim, *Appl. Phys. Lett.*, 1999, **75**, 3129.
- 2 K.B.K. Teo, E. Minoux, L. Hudanski, F. Peauger, J.P. Schnell, L. Gangloff, P. Legagneux, D. Dieumegard, G.A.J. Amaratunga, W.I. Milne, *Nature*, 2005, **437**, 968.
- 3 J. Zhang, G. Yang, Y. Cheng, B. Gao, Q. Qiu, Y.Z. Lee, J.P. Lu, O. Zhou, *Appl. Phys. Lett.*, 2005, **86**, 184104.
- 4 N. de Jonge, Y. Lamy, K. Schoots, T.H. Oosterkamp, *Nature*, 2002, **420**, 393.
- 5 F.G. Rüdener, *Surf. Interface Anal.*, 2007, **39**, 116.
- 6 W.A. de Heer, A. Châtelain, and D. Ugarte, *Science*, 1995, **270**, 1179.
- 7 I. Lahiri, R. Seelaboyina, J.Y. Hwang, R. Banerjee, W. Choi, *Carbon*, 2010, **48**, 1531.
- 8 P.G. Collins, and A. Zettl, *Appl. Phys. Lett.*, 1996, **69**, 1969.
- 9 Q.H. Wang, A.A. Setlur, J.M. Lauerhaas, J.Y. Dai, E.W. Seelig, R.P.H. Chang, *Appl. Phys. Lett.*, 1998, **72**, 2912.
- 10 H. Dai, *Accounts Chem. Res.*, 2002, **35**, 1035.
- 11 C. Indrani, and A. Pushan, *Nanotechnology*, 2012, **23**, 015704.
- 12 A. Dangwal, C. S. Pandey, G. Müller, S. Karim, T. W. Cornelius, C. Trautmann, *Appl. Phys. Lett.*, 2008, **92**, 063115.
- 13 F. Maurer, A. Dangwal, D. Lysenkov, G. Müller, M. Eugenia Toimil-Molares, C. Trautmann, J. Brötz, H. Fuess, *Nuclear Instruments and Methods in Physics Research*, 2006, **245**, 337.
- 14 C.J. Lee, T.J. Lee, S.C. Lyu, Y. Zhang, H. Ruh, H.J. Lee, *Appl. Phys. Lett.*, 2002, **81**, 3648.
- 15 Y. Alivov, M. Klopfer and S. Molloy, *Appl. Phys. Lett.*, 2011, **99**, 063104.
- 16 S.C. Yeon, W.Y. Sung, W.J. Kim, S.M. Lee, H.Y. Lee, Y.H. Kim, *Journal of Vacuum Science & Technology B*, 2006, **24**, 940.
- 17 R.Z. Zhan, J. Chen, S.Z. Deng, N.S. Xu, *Journal of Vacuum Science & Technology B*, 2010, **28**, 558.
- 18 I. Lahiri, J. Wong, Z. Zhou, W. Choi, *Appl. Phys. Lett.*, 2012, **101**, 063110.
- 19 Z. Yan, L. Ma, Y. Zhu, I. Lahiri, M.G. Hahm, Z. Liu, S. Yang, C. Xiang, W. Lu, Z. Peng, Z. Sun, C. Kittrell, J. Lou, W. Choi, P.M. Ajayan, J.M. Tour, *ACS Nano*, 2012, **7**, 58.
- 20 N. Liu, G. Fang, W. Zeng, H. Long, X. Zhao, *The Journal of Physical Chemistry C*, 2011, **115**, 14377.
- 21 Y. Liu, Y. Xie, J. Chen, J. Liu, C. Gao, C. Yun, B. Lu, E. Xie, *J. Am. Ceram. Soc.*, 2011, **94**, 4387.
- 22 I. Lahiri, and W. Choi, *Acta Mater.*, 2011, **59**, 5411.
- 23 W. Zhang, S. Ding, Z. Yang, A. Liu, Y. Qian, S. Tang, S. Yang, *J. Cryst. Growth*, 2006, **291**, 479.
- 24 C.T. Hsieh, J.M. Chen, H.H. Lin, H.C. Shih, *Appl. Phys. Lett.*, 2003, **83**, 3383.
- 25 J. Chen, S.Z. Deng, N.S. Xu, W. Zhang, X. Wen, S. Yang, *Appl. Phys. Lett.*, 2003, **83**, 746.
- 26 X. Xue, P. Deng, S. Yuan, Y. Nie, B. He, L. Xing, Y. Zhang, *Energy & Environmental Science*, 2013, **6**, 2615.
- 27 U. Husnu Emrah, and C. Manish, *Nanotechnology*, 2005, **16**, 2153.
- 28 E.F. Antunes, A.O. Lobo, E.J. Corat, V.J. Trava-Airoldi, A.A. Martin, C. Verissimo, *Carbon*, 2006, **44**, 2202.

- 27 Lahiri, I., V.P. Verma, and W. Choi, *Carbon*, 2011, **49**, 1614.
- 28 I. Lahiri, D. Lahiri, S. Jin, A. Agarwal, W. Choi, *ACS Nano*, 2011, **5**, 780.
- 29 J. L. Qi, X. Wang, W. T. Zheng, H. W. Tian, C. Q. Hu, Y. S. Peng, *J.Phys. D: Appl. Phys.*, 2010, **43**, 055302.
- 30 U. A. Palnitkar, R. V. Kashid, M. A. More, Dilip S. Joag, L. S. Panchakarla, C. N. R. Rao, *Appl. Phys. Lett.*, 2010, **97**, 063102.
- 31 I. Lahiri, R. Seelaboyina, J. Y. Hwang, R. Banerjee, W. Choi, *Carbon*, 2010, **48**, 1531.
- 32 R. B. Sharma, D. J. Late, D. S. Joag, A. Govindraj, C. N. R. Rao, *Chem. Phys. Lett.*, 2006, **428**, 102.
- 33 Y. Shiratori, K. Furuichi, S. Noda, H. Sugime, Y. Tsuji, Z. Zhang, S. Maruyama, Y. Yamaguchi, *Jpn. J. Appl. Phys.*, 2008, **47**, 4780.
- 34 C. Kimura, T. Yamamota, S. Funakawa, M. Hirakawa, H. Murakami, T. Sugino, *J. Vac. Sci. Technol. B*, 2012, **21**, 2212.
- 35 T. Sugino, C. Kimura, T. Yamamota, *Appl. Phys. Lett.*, 2002, **80**, 3602.
- 36 Zhi Xu, X. D. Bai, E. G. Wang, *Appl. Phys. Lett.*, 2006, **88**, 133107
- 37 A. Mayer, N. M. Miskovsky, P. H. Cutler, *Phys. Rev. B*, 2011, **65**, 155420.